Pesquisa Antártica Brasileira (2004) 4: 57-65
(Brazilian Antarctic Research)
ISSN 0103-4049
www.cnpq.br/areas/terra_meioambiente/proantar/

High-resolution radar mapping of internal layers of a subpolar ice cap, King George Island, Antarctica

JANDYR M. TRAVASSOS[1] **and JEFFERSON C. SIMÕES**[2]

[1]Observatório Nacional – CNPq, Rua Gen. José Cristino 771, 20921-400 Rio de Janeiro, RJ, Brasil
[2]Núcleo de Pesquisas Antárticas e Climáticas, Departamento de Geografia
Universidade Federal do Rio Grande do Sul – 91501-970 Porto Alegre, RS, Brasil

ABSTRACT

A GPR survey was carried out to investigate the structure and hydrology of King George Island subpolar ice cap, Antarctica. This study was part of a larger investigation on the mass balance of Lange Glacier (62°07'S, 58°36'W), an outlet ice mass that is receding. The strongest signal in all reflection profiles is due to the presence of free water. Sections show strong near-surface reflectors sitting on weaker ones above the water table. Below the water table, reflectors become strong again, displaying many discrete events that reach the end of the sections. Varying antenna configuration causes an important distinction in radar response for the same subsurface. A nearby snow and ice core was used to calibrate the top section of the GPR images.

Key words: ground penetrating radar, glaciohidrology, glacier geophysics, internal reflectors.

INTRODUCTION

The GPR (Ground Penetrating Radar) technique is a common tool for the exploration of cold regions due to the excellent penetration of radio waves in ice and frozen ground. This is because, in contrast to most materials, cold ice is relatively transparent to radar waves. In fact, over the last three decades, radio echo devices and radar systems have been developed for a variety of large-scale applications in Glaciology. Deep penetrating radar has been used to map the bedrock beneath glaciers and ice sheets to depths as great as several kilometers (*e.g.*, Bogorodsky et al. 1985). These systems are operated on the ice surface or are airborne.

GPR has been used in Glaciology to image ice stratigraphy (Arcone et al. 1995, Arcone 1996, Murray et al. 1997), to determine accumulation rates by interpreting reflecting horizons in Antarctic firn (Forster et al. 1991), and on temperate glaciers (Kohler et al. 1997). GPR has also been used for inferring the dielectric properties of near-surface snow, firn and ice that are important for interpreting SAR satellite images (Rott et al. 1993). In addition, due to small permittivity changes within the ice, GPR data can also be used to give direct measurements of ice thickness, bedrock topography, and to display many internal reflections between the bedrock and ice surface. They can be used in the determination of the mass balance of ice sheets that, along with their size and dynamics, are key issues in assessing the effect of global climate change (Paterson 1994, van der Veen 1991). Even large volcanic events may be detected in GPR sections (Millar 1981).

The present work is part of a larger study investigating the mass balance of Lange Glacier (62°7'S, 58°36'W), an outlet glacier in southern of King George Island. This glacier has receded about 1 km since 1956, probably due to regional warm-

Correspondence to: Jandyr M. Travassos
E-mail:jandyr@on.br

ing (Aquino 1999 unpublished). The average temperature at King George Island has increased 1.1°C from 1947 to 1995 (Ferron et al. 2004, this volume). The King George Island subpolar ice field, above 600 m of altitude, is near the pressure melting point throughout. It is known that the ice cover is thicker than 300 m (Macheret and Moskalevsky 1999, Pfender 1999).

SITE DESCRIPTION

King George Island is the largest of the South Shetland Islands, near the northern tip of the Antarctic Peninsula. Its ice cap is discharged to the sea by a series of tidewater outlet glaciers. Lange Glacier is one of these outlet glaciers. It has an area of 28.3 km^2, terminating in Admiralty Bay (Figure 1). Data were collected in the summer of 1997/1998, along two traversing breadth profiles. A few smaller profiles were taken on an ice dome nearby. This work will concentrate on the larger profile, which covered 1,268 m, stopping short of the many crevasses in the area (Figure 1), and on three short profiles. The shorter profiles, 80 m long, were deployed on a 300 m thick ice dome (Collins Dome), at about 600 m a.s.l. (Macheret and Moskalevsky 1999, Pfender 1999), Figure 1. A 49.9 m deep ice core was drilled one year before this survey (Simões et al. 2004, this volume).

EQUIPMENT AND FIELD PROCEDURES

The radar system was a PULSE EKKO IV with bistatic unshielded 50 MHz antennae with a 50 MHz pulse bandwidth. We have used a 100 V pulser with a 6 ns rise time, best suited for the relatively low frequency used. The center frequencies should yield short duration wavelets and tightly confined high gain radiation patterns. The antennae were dragged by hand and by snowmobile, and they were kept 2 m apart for the fixed-offset profiles. We tested both broadside perpendicular (BPer) and parallel (BPar) antennae configurations for the hand-dragged profiles. In the BPer configuration, the antennae were deployed perpendicular to the profile direction, whereas for the BPar configuration, they were kept parallel to the profile direction.

We used manual triggering for the hand-dragged profiles. We collected GPR data along three 80 m long profiles, deployed as a bisected L. These profiles were done to:

1) compare ice signatures for both BPer and BPar antennae configurations,
2) analyze the reading/recording performance of the GPR-Laptop system for the snowmobile dragged profiles,
3) calibrate the shallow portions of the GPR images using the results of the borehole, and
4) estimate ice velocity by means of a CMP profile.

Data were collected with 50 MHz antennae, a time window of 2040 ns (the maximum allowed by the equipment) and a sampling rate of 1.6 ns. The adopted step size was 0.5 m for the fixed offset and 0.2 m for the CMP schemes. A relatively high stack of 16 was used throughout the survey. Seven fixed-offsets and one CMP GPR profiles were deployed on the L-shaped field layout (Travassos and Simões 1999).

The findings from the hand-dragged profiles were used to set the parameters for the snowmobile dragged fixed offset profiles. We found the data acquisition rate heavily dependent on the sampling interval for a given towing speed and time window. Positioning was provided by a post-processed differential GPS, a pair of Magellan ProMark X. We expected a 1 m positioning and a 2 m height accuracy, with 1 s readings. The GPS was mounted on the snowmobile towing two Nansen sledges, the first, with the GPR console and the second one, with the antennae. The antennae sledge was 20 m away from the snowmobile. Figure 2 shows the snowmobile train used for the fixed-offset profiles.

We used automatic data collection for the snowmobile dragged fixed offset profiles. The GPR spatial sampling is a compromise between the speed of the snowmobile and the recording capability of

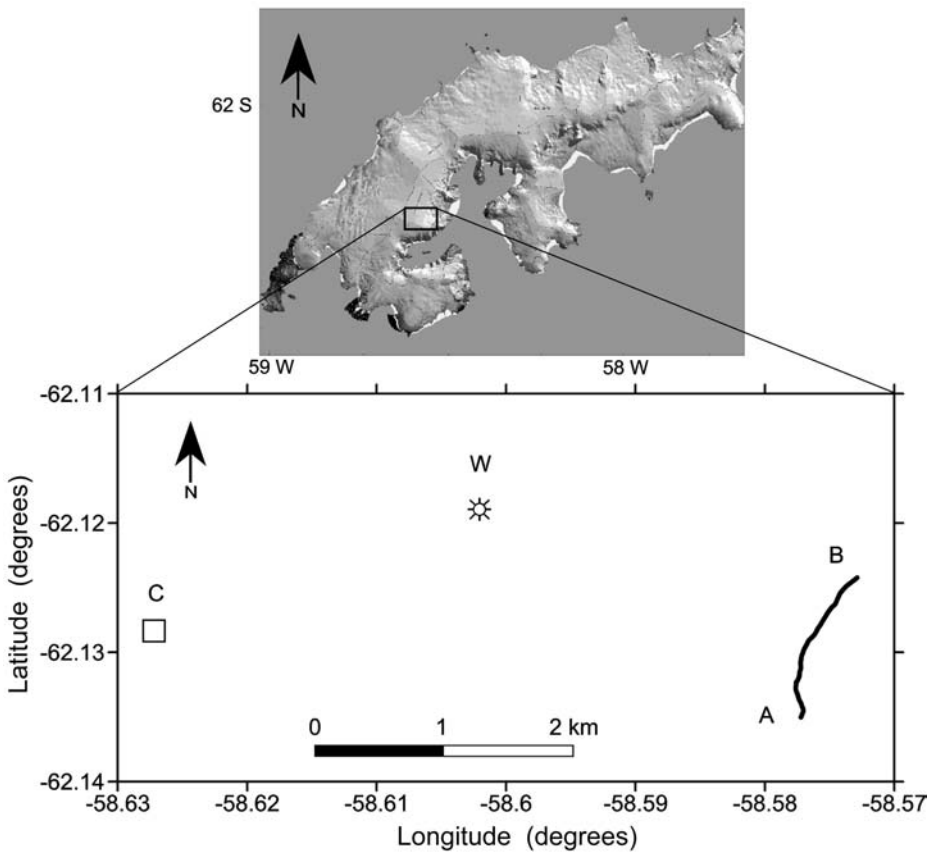

Fig. 1 – The upper panel shows a map of King George Island. The small rectangle shows the location of the surveyed area. The lower panel is a blow up of the survey area. The main GPR profile is marked AB, the area of the smaller profiles is marked C, and the borehole location is W.

the system GPR-Laptop. The median speed of towing was 3.8 m s^{-1}. We expected a spatial sampling of 0.7 m for the GPR-Laptop system, and with the following field settings: a time window of 2040 ns, a sampling interval of 4 ns and a relatively lower stack of 4. The actual spatial sampling was later found to be a fractional figure just under 0.9 m that was later set to 1 m.

Antennae Configurations

The 3 shorter profiles deployed in the bisected L-shaped field layout were done several times with BPer and BPar antennae configurations, in order to investigate any directional dependence as well as any correlation to the internal structure of the glacier that may exist. Profiles done with the BPer configuration produce a crisscrossing pattern due the interference of closely spaced diffractions, a behavior not seen using the BPar configuration, Travassos and Simões (1999), (Figure 3). Such behavior should be expected in cluttered environments like temperate glaciers (Moran et al. 2000, Watts and England 1976).

The noise observed in the BPer data is probably generated by diffractions from inclusions of water-filled voids and debris in the ice (Smith and Evans 1972, Watts and England 1976). This clutter severely limits the effectiveness of a radar survey. The BPar data appear to be less noisy, free of a crisscrossing pattern. Such behavior was reported else-

Fig. 2 – Snowmobile train for the common-offset profiles. The GPS antenna is mounted on the snowmobile. The GPR console is mounted on a Nansen sledge, next to the snowmobile, and the antennae on a second sledge some 15 m away form the first sledge. The antennae are securely tied to the bottom part of the sledge as seen in the inset. The large picture was taken on Lange Glacier, looking SE towards Admiralty Bay.

where (Nobes 1999, Travassos and Simões 1999), but this does not imply that the BPar data may be noise-free. In fact, the resolving power of BPar data is less than the migrated BPer data, as seen in Figure 3. Due to noise, several ice reflectors seen in the BPer section are missing in the BPar one. For instance, the BPer (A and C) reflector, at 250 ns, is not seen in the BPar section (B). This picture does not change if we do other profiles, changing measuring direction. Irrespective of profile direction, we obtain the same results, ruling out a directional anisotropy in the ice as a cause for the observed noise. In this work, we will use the migrated BPer data to interpret ice structure, eventually reaching the basal zone on the longer profile.

The theoretical transmit directivities and footprint for an unshielded, finite-size loaded dipole operating monostatically on a homogeneous half-space of ice are useful to understand the GPR images obtained in this work. They can be easily found in the literature (Arcone 1995). For the purposes of this work, it is important to keep in mind that the radiation pattern on the H-field plane, a vertical plane perpendicular to the antenna axis, has maximum intensity in two shell-like lobes. This makes

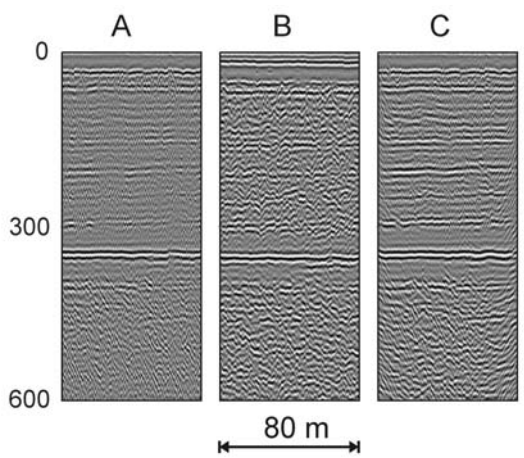

Fig. 3 – The three panels of this figure show the same 80-m long profile data obtained with BPer (A), BPar (B) and migrated BPer (C) antennae configurations. All the data was high-pass filtered (40% of Nyquist). We adopted an ice velocity of 0.194 m ns^{-1} (see text). Note the BPer (A and C) reflector at 250 ns, which is not seen in the BPar section (B). The total time span is restricted to 600 ns, a penetration depth of more than 50 m.

the footprint, along the profile direction of a broadside-perpendicular configuration, roughly twice as long as the perpendicular direction, at any given depth (Arcone 1995). This footprint pattern indicates that sensitivity is greater along the H-field plane. The footprint pattern associated with the cone of irradiated energy, which has apertures well above 90°, indicates that diffractions in ice can have asymptotes with higher signal strengths than their apexes. Conversely, a BPar configuration does not show the diffractions within the ice, but, on the other hand, is not immune to the clutter. The best results are obtained collapsing the diffractions, via migration, to clear out the diffractions in the BPer data.

DATA PROCESSING

Data processing included high-pass filtering, 40% of Nyquist, and 2-D Stolt migration. The reader should be aware that depth estimates could give rise to substantial errors when applied to a steeply dipping glacier bed.

Ice velocity was estimated, via a 50 m long CMP profile, with the antennae moved by hand in a Bper configuration. The CMP profile was done along the same profile direction as the one shown in Figure 3. Velocity in the ice was estimated through stacking after move out correction yielding 0.19 m ns^{-1}. This should be considered a first estimate for the velocity model in the area. Here, we adopt a two-layer velocity model found elsewhere (Pfender 1999). Here, we will assume that the velocity found in our CMP profile holds down to 350 ns, where we found a main water body (Travassos and Simões 1999). We adopted the value of 0.168 m ns^{-1} from that depth down (Bogorodsky et al. 1985, Paterson 1994). Depths can then be found by:

$$\begin{aligned} Z &= 0.095t \\ &\quad (m \text{ and } t \text{ in } ns; t < 350\, ns) \\ Z &= 33.25 + 0.084\,(t - 350) \\ &\quad (m \text{ and } t \text{ in } ns;\ \text{otherwise}) \end{aligned} \tag{1}$$

RESULTS

Borehole Log Data and Resolution Power

This paper uses the results from a 49.7 m long ice core, drilled one year before the GPR survey, Figure 1. The ice core revealed a high number of thin layers ranging from 1 mm wind crusts to 4 cm ice layers. Somewhat thicker layers of 6-20 cm were found in the core. Coarse grain layers, thicker than 1.15 m, were also reported. The issue here is to assess whether thin stratigraphic horizons, like the ones observed in the core, are detectable with the GPR wavelet.

The vertical resolution of the GPR data is determined by the bandwidth center frequency wavelength. For the 50 MHz configuration used here, and for the estimated phase velocity of the electromagnetic field in the glacier, the practical wavelength is $\lambda = 3.8$ m. The level of detectability of a given ice horizon will be a function of this wavelength and of the signal-to-noise ratio. As the layers become thinner, the reflected energy becomes a composite of the reflections on both interfaces. The two reflections combine in a way that there is still enough energy to detect the layer, although it is not possible to resolve its thickness b. In the absence of noise, this happens at $b = \lambda/8$ (Widess 1973). Thin beds of $b = \lambda/20$ should be detectable with an amplitude of about 60% of a thick bed, at the same depth (Widess, 1973). On the other hand, destructive interference can render a not so thin layer of $b = \lambda/2$, just under 2 m, which is transparent to radar (Rossiter et al. 1975, Widess 1973).

In this work, a theoretically detectable thin bed falls in the range of $b = [0.02, 0.48]$ m. Density measurements were made every 11 cm, along the ice core. This allows for resolving a given layer if it is at least 22 cm thick. In terms of density measurements, about 39% of the recognizable layers in the ice core fall in the category of a thin layer, i.e., between 22 and 48 cm. This is important information as ice density and radar velocities are related to each other (Paterson 1994). Thicker layers account for 8% of the total.

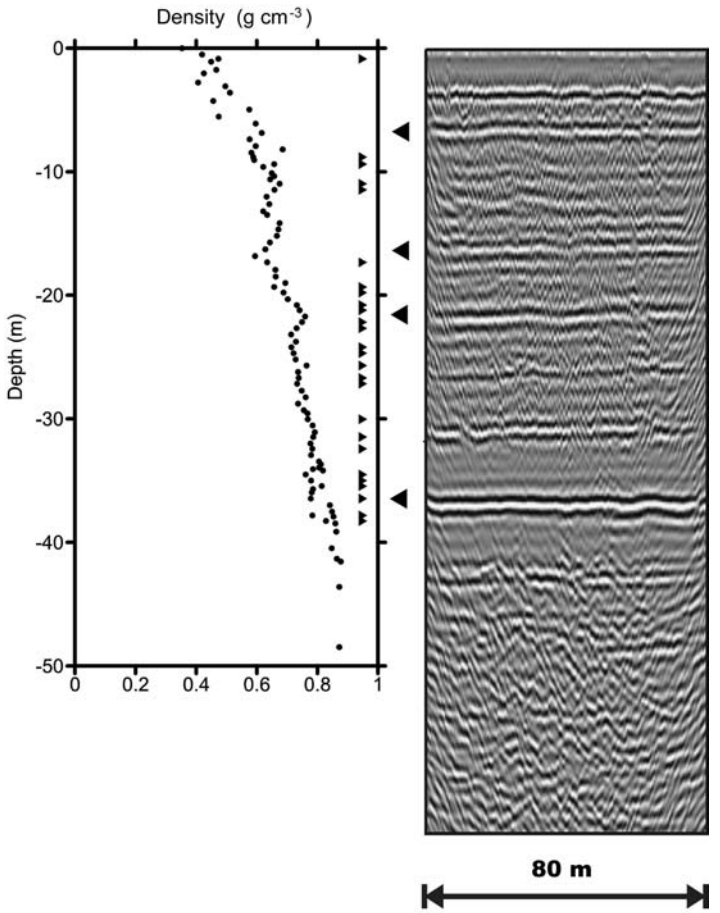

Fig. 4 – The left panel shows the density log from the ice core (W in Figure 1). Density values are shown as black dots. Small right pointing arrowheads show the depths of detectable thin layers. Larger left pointing arrowheads show where reflectors clearly correlate to changes in density. The right panel is the migrated BPer GPR section (panel C in Figure 3).

We can compare the GPR and ice core data in order to calibrate the shallower parts of the GPR sections. This is done comparing the migrated BPer GPR long profile (section C in Figure 3) with the borehole log data. Figure 4 brings the density log and the GPR data side by side. The same figure shows the depths of the detectable thin layers. A main body of water was found in the borehole about 37 m deep. The water occurs within a coarse grain firn level about 1 m thick. The GPR detects the water table at 33 m as a clear change in polarity. This discrepancy is consistent with the difference in height between the surveyed area and the borehole. Note that the transition between firn and ice occurs at the density of 0.830 g cm^{-3}. Several other reflectors correlate well with changes in density. A few thin layers appear to correlate to a given reflector.

Profile AB

The results of this profile were high-pass filtered, but not migrated, in order to leave the diffractions caused by large inhomogeneities in the ice. The results are in Figure 5. The section shows a top layer of snow and firn that ends on the top of the ice, at about 400 ns, or 38 m. The presence of water on that interface is clear. The crisscrossing pattern is

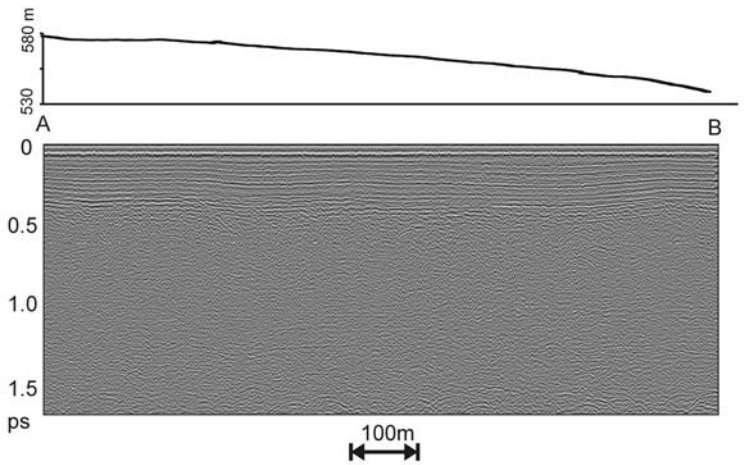

Fig. 5 – The bottom panel shows the GPR profile AB. The vertical axis reaches 1.7 ps (1700 ns). The upper panel shows the topography along the profile. There is a 40 m change in elevation between A and B.

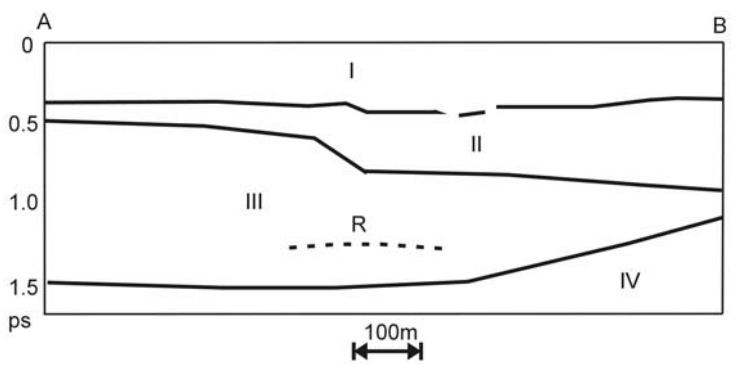

Fig. 6 – Interpretation of profile AB. The GPR section can be subdivided into four zones based on radar response. Snow and firn layers are in Zone I. Free water is conspicuous on the interface between Zones I and II. Zone II displays large diffractions in ice becoming uniform in Zone III. R is a reflector within Zone III. Diffractions appear again in Zone IV, due to a complex glacier bed.

clear above the interface. The section changes dramatically below it. Large diffractions indicate that the ice is highly inhomogeneous, probably due to pockets of water. These pockets are probably much larger than the voids seen above 38 m. The larger diffractions are more numerous on the second half of the section. These pockets tend to disappear with depth. The ice shows some evidence of layering, but reflectors do not run for the whole section. Below 1300 ns, diffractions appear again but now due to the bedrock of the glacier. Such diffractions have their apexes around or below 1400 ns, or 130 m. The evidence points to a complex glacier bed.

The GPR section AB can be roughly subdivided in 4 zones, as shown in Figure 6. Snow and firn layers are in Zone I. This zone is characterized by noise in the form of a crisscrossing pattern, due the interference of closely spaced diffractions from water-

filled voids and debris inclusions. Free water is conspicuous on the interface, between Zones I and II. Zone II is characterized by larger diffractions, indicating a highly inhomogeneous ice, probably having many water filled pockets. Ice becomes uniform in Zone III, this allows for the appearance of reflectors like R. Diffractions appear again in Zone IV, due to a complex glacier bed.

CONCLUSIONS

The GPR data, analyzed here, displayed high levels of glaciological noise, probably due to voids and debris inclusions in ice, an expected feature of a glacier at the pressure melting point. Although BPar antennae configuration is less sensitive to this noise, one must use BPer configuration, as it is more accurate in revealing ice structure. Ice velocity was 0.19 m ns^{-1} at least for the first 50 m. Sections correlated well with an ice core drilled one year before the survey. This allowed for the calibration of the shallow parts of the sections. The most conspicuous feature in the sections was the reflection from a water body, 30 m below the surface. The presence of larger inhomogeneities was seen below the water table, probably due to pockets filled with water. The sections end with diffractions indicating a complex glacier bed.

ACKNOWLEDGMENTS

The Brazilian Antarctic Program (PROANTAR) and the Brazilian National Council for Scientific and Technological Development (CNPq) provided the funding for this research. JM Travassos and JC Simões were supported by CNPq grants. Special thanks go to Dr. Augusto CB Pires of the University of Brasilia (UnB) who kindly lent the GPR equipment used in this work.

RESUMO

Um levantamento por GPR (Geo-radar) foi realizado para investigar a estrutura e hidrologia da calota de gelo sub polar da ilha Rei George, Antártica. Este estudo foi parte de uma investigação mais ampla sobre o balanço de massa da geleira de descarga Lange (62°07'S, 58°36'W), a qual está retraindo. O sinal mais forte em todos os perfis de reflexão é devido à presença de água livre. As seções mostram refletores fortes perto da superfície e situados sobre outros mais fracos acima de um aqüífero. Abaixo deste aqüífero, as reflexões tornam-se fortes novamente, mostrando muitos eventos distintos e que alcançam o final das seções. A variação na configuração das antenas causa diferenças importantes na resposta do radar para uma mesma subsuperfície. Um testemunho de neve e gelo obtido nas proximidades foi usado para calibrar a seção superior das imagens GPR.

Palavras-chave: Geo-radar, glaciohidrologia, geofísica de geleiras, refletores internos.

REFERENCES

AQUINO FE. 1999. Sedimentação moderna associada à Geleira de Maré Lange. Porto Alegre: Universidade Federal do Rio Grande do Sul, 106 p. Unpublished M.Sc. dissertation.

ARCONE SA. 1995. Numerical studies of the radiation patterns of resistively loaded dipoles. J App Geophys 33: 39–52.

ARCONE SA. 1996. High resolution of glacial ice stratigraphy: a ground-penetrating radar study of Pegasus Runway, McMurdo Station, Antarctica. Geophysics 61: 1653–1663.

ARCONE SA, LAWSON DE AND DELANEY AJ. 1995. Short-pulse radar wavelet recovery and resolution of dielectric contrasts within englacial and basal ice of Matanuska Glacier, Alaska, U.S.A. J Glaciol 41: 68–86.

BOGORODSKY VV, BENTLEY CR AND GUDMANDSEN PE. 1985. Radioglaciology. Dordrecht: Reidel, 254 p.

FERRON FA, SIMÕES JC, AQUINO FE AND SETZER AW. 2004. Air temperature time series for King George Island, Antarctica. Pesq Antart Bras 4: 155–169.

FOSTER R, DAVIS C, RAND T AND MOORE RK. 1991. Snow-stratification investigation on an Antarctic ice stream with an X-band radar system. J Glaciol 37: 323–325.

KOHLER J, MOORE JC, KENNET M, ENGESET R AND ELVEHOY H. 1997. Using ground-penetrating radar to image previous years' summer surfaces for mass-balance measurements. Ann Glaciol 24: 355–360.

MACHERET YYA AND MOSKALEVSKY YUYA. 1999. Study

of Lange Glacier on King George Island, Antarctica. Ann Glaciol 29: 202–206.

MILLAR DHM. 1981. Radio-mho layering in polar ice sheets and past volcanic activity. Nature 292: 441–443.

MORAN ML, ARCONE SA AND DELANEY AJ. 2000. Delineation of a temperate glacier bed using 3-D migration. In: INTERNATIONAL CONFERENCE ON GROUND PENETRATING RADAR (GPR2000), 8., Dordrecht. Proceedings CD-Rom..., Dordrecht, 2000, paper Moran02, 6 p.

MURRAY T, GOOCH DL AND STUART GW. 1997. Structures within the surge front at Bakaninbreen, Svalbard, using ground-penetrating radar. Ann Glaciol 24: 122–129.

NOBES DC. 1999. The directional dependence of the ground penetrating radar response on the accumulation zones of temperate alpine glaciers. First Break 17: 249–259.

PATERSON WSB. 1994. The Physics of Glaciers. Oxford: Elsevier, 480 p.

PFENDER M. 1999. Topographie und Glazialhydrologie von King George Island, Antarktis. Münster: Westfälischen Wilhelms-Universität Münster, 99 p. Diplomarbeit im Fach Geophysik.

ROSSITER JR, STRANGWAY DW, ANNAN AP, WATTS RD AND REDMAN JD. 1975. Detection of thin layers by radio interferometry. Geophysics 40: 299–308.

ROTT H, STURM K AND MILLER H. 1993. Active and passive microwave signatures of Antarctic firn by means of field measurements and satellite data. Ann Glaciol 17: 337–343.

SIMÕES JC, FERRON FA, BERNARDO RT, ARISTARAIN AJ, STIÉVENARD M, POURCHET M AND DELMAS RJ. 2004. Ice core study from the King George Island, South Shetlands, Antarctica. Pesq Antart Bras 4: 9–23.

SMITH BME AND EVANS S. 1972. Radio echo sounding: absorption and scattering by water inclusions and ice lenses. J Glaciol 11: 133–146.

TRAVASSOS JM AND SIMÕES JC. 1999. Stratigraphy and hydrology of a subpolar ice field, King George Island. In: INTERNATIONAL CONGRESS OF THE BRAZILIAN GEOPHYSICAL SOCIETY, 6., Rio de Janeiro. Annals CD-Rom..., Rio de Janeiro. Expanded Abstract.

VAN DER VEEN CJ. 1991. State of balance of the cryosphere. Rev Geophys 29: 433–455.

WATTS RD AND ENGLAND AW. 1976. Radio-echo sounding of temperate glaciers: ice properties and sounder design criteria. J Glaciol 17: 39–48.

WIDESS MB. 1973. How thin is a thin bed? Geophysics 38: 1176–1180.